Chalcogenide Letters Vol. 19, No. 12, December 2022, p. 939 - 953

Multicomponent Ge-As-Te-Pb chalcogenide glasses for radiations shielding applications

M. Ezzeldien[a*], M. A. Salama[b], M. F. Hasaneen[a], A. A. El-Maaref[a], M. M. Soraya[c,d], N. M. Shaalan[e,f], Z. A. Alrowaili[a], M. Ahmad[g,h]
[a] *Department of Physics, College of Science, Jouf University, Al-Jouf, Sakaka, P.O. Box 2014, Sakaka, Saudi Arabia*
[b]*Deanship of Common First Year, Jouf University, P.O.Box 2014 Sakaka, KSA*
[c]*Physics Department, Faculty of Science, Aswan University, Aswan, Egypt*
[d]*Academy of Scientific Research and Technology (ASRT), Egypt*
[e]*Department of Physics, College of Science, King Faisal University, P.O. Box 400, Al-Ahsa 31982, Saudi Arabia*
[f]*Physics Department, Faculty of Science, Assiut University, Assiut 71516, Egypt*
[g]*Department of Physics, Collage of Science in Zulf, Majmaah University, Majmaah 11952, Saudi Arabia*
[h]*Physics Department, Faculty of Science, Al-Azhar University, Assiut 71452, Egypt*

Phy-X/PSD online program is used to obtain various radiation shielding indices in a photon energy region located between 0.15 and 15 MeV for Ge_{25}-As_{10}-Te_{65-x}-Pb_x (x = 2, 4, 6, 8, 10 at %) chalcogenide glasses. The linear attenuation coefficient LAC, mass attenuation coefficients MAC, effective atomic number Z_{eff}, effective electron density N_{eff}, half-value layer, HVL, tenth value layer TVL, mean free path MEF, energy absorption and exposure buildup factors (EABF, EBF), and fast neutron cross section FNRCS have been introduced. The findings conclude that the LAC and MAC measurements are greater and therefore better than commercial and traditional glasses. Also, it was found that HVL, TVL, and MFP were reduced with the addition of Pb to the tested glasses, which improve the shielding characteristics. Z_{eff} and N_{eff} of the compositions under study were varied as (42.58- 59.75) and (2.36-3.09 x 10^{23} electrons/g) respectively. A reduction was noticed in EBF and EABF values with the increment of Pb concentration in the investigated glasses at the entire photon energies, at all values of MFP that emphasize the enhancement of shielding properties of these glasses with the addition of lead. FNRCS were found to be changed between 0.87 and 0.095 Cm^{-1} as Pb content varies from 0.0 to 0.01 respectively that let these glasses considered to be better as neutrons shield than some ordinary and commercial glasses.

(Received August 23, 2022; Accepted December 13, 2022)

Keywords: Chalcogenide glass, Ge-As-Te-Pb, Shielding coefficients, Radiations shielding, Phy-X/PSD program

1. Introduction

Ionizing radiation is one of energy types emitted by specific atoms in the form of electromagnetic waves or particles. Those who get exposed to ionizing radiation natural sources, including what is found in water, plants and soil, as well as man-made sources e.g. X-ray machines and medical devices. Ionizing radiation is beneficial in some ways, since it is utilized in fields e.g. industry, medicine, agriculture and scientific research. As the use of ionizing radiation increases, the potential for health risks increases if it is not contained or used in a proper way. Severe health impacts such as acute radiation syndrome, or skin burning can happen when radiation doses exceed certain levels. To prevent the harmful effects of these radiations has become an urgent

Corresponding author: meabas@ju.edu.sa
https://doi.org/10.15251/CL.2022.1912.939

necessity especially for workers who deal with high doses of high energies radiations. The most investigated materials were concretes, polymers, rocks and alloys [1-7]. The good competition between the various shielding compositions is mainly done based on different factors including efficiency, low cost, flexibility, transparency, and toxicity. Recently, many scientists have developed various shielding materials [8-16]. The oxide glasses have the most of these efforts, because of their great shielding efficiency, their high transparency and low manufacturing costs.

Nowadays, chalcogenide glasses are studied as shielding materials by many researchers as their shielding characteristic is expected to be better than oxide glasses since they are denser [17-19]. The investigation of chalcogenides as shielding radiations is resulted in recognizing that they are better than many other traditional, commercial glasses and oxide glasses [17-19]. The stability of these materials against high energetic radiations is enhancing their usage as shielding materials [20]. Theoretically, many programs have been used to investigate the shielding indices. These programs include XCOM and Monte Carlo simulation codes [21–27]. Phy-X/PSD online software has been recently developed for this purpose [13]. Upon Phy-X/PSD, many research papers have been published in various respectful journals [18, 28, 29]. In the present study we aim to determine the shielding factors of Ge_{25}-As_{10}-Te_{65-x}-Pb_x (x = 0, 2, 4, 6, 8, 10 at %) according to Phy-X/PSD online program in a photon energy region located between 0.15 and 15 MeV, compare the results of the various shielding parameters with those of the ordinary and commercial glasses, discuss the findings according to the physical properties of these materials and indicate the possibility of using these materials as materials with high radiation protection.

2. Materials and methods

It has been confirmed that the ability of synthesizing the multicomponent chalcogenide glasses Ge_{25}-As_{10}-Te_{65-x}-Pb_x, and their interesting physical properties were investigated [30]. the Shielding characteristics of Ge_{25}-As_{10}-Te_{65-x}-Pb_x are our focus of interest. The Phy-X/PSD program is used to evaluate the radiation shielding indices in the photon energy located through 0.015 and 15 MeV. The density and the corresponding chemical formula of each investigated sample were inputted. Then the program has been calculated the shielding factors. As it is known, the time taken to complete these calculations depends on the number of the investigated samples and the used computer processor. We have used a laptop of processor intel (R) core (TM) i7-10750H CPU @ 2.6 GHz. Table 1 shows the various compositions under investigation, their abbreviations, and the corresponding densities (gm/Cm^3).

Table 1. The abbreviations and densities of Ge_{25}-As_{10}-Te_{65-x}-Pb_x (x = 0, 2, 4, 6, 8, 10 at %) compositions.

Sample no.	Name	Code	Density
1	Ge_{25}-As_{10}-Te_{65}	GATP1	6.033
2	Ge_{25}-As_{10}-Te_{63}-Pb_2	GATP2	6.216
3	Ge_{25}-As_{10}-Te_{61}-Pb_4	GATP3	6.394
4	Ge_{25}-As_{10}-Te_{59}-Pb_6	GATP4	6.566
5	Ge_{25}-As_{10}-Te_{57}-Pb_8	GATP5	6.735
6	Ge_{25}-As_{10}-Te_{55}-Pb_{10}	GATP6	6.899

The well-recognized Beer-Lambert formula that identifies the relation between the attenuated, I and un-attenuated, I_o as a mono-energetic photon intensities migrating across the medium is defined as [31]:

$$I = I_0 e^{-\mu d} \tag{1}$$

where μ (cm^{-1}) is the linear attenuation coefficient, and d (in cm) is the thickness. The mass attenuation coefficient, MAC (μ_m, in cm^2/g) is a parameter defining the likelihood of interactions, between the incident photons and the mass of an area equal unity for a material [31]:

$$\mu_m = \left(\frac{\mu}{\rho}\right) = - \frac{\ln(I/I_0)}{\rho d} = - \frac{\ln(I/I_0)}{d_m} \tag{2}$$

where d_m (in g/cm^2) is the mass thickness of a specimen, and ρ (g/cm^3) is the density of the material. The next expression evaluates the μ_m for a certain sample [31]

$$\mu_m = \left(\frac{\mu}{\rho}\right) = \sum_j w_j \left(\frac{\mu}{\rho}\right)_j , \tag{3}$$

where w_j is the weight fraction of the j^{th} involved element. The half-value layer *HVL* and the tenth value layer *TVL* are the essential depth to lower the intensity of the incident photons to 0.5 and 0.1 of its value, respectively [13].

$$HVL = \frac{\ln(2)}{\mu} \ , \ TVL = \frac{\ln(10)}{\mu} , \tag{4}$$

The mean free path *MFP*, distinguish the mean distance the photons travel before making a further interaction and estimated according to μ values as followed [13]:

$$MFP = \frac{1}{\mu} , \tag{5}$$

The effective atomic number Z_{eff} of the material based on the next formula [13]:

$$Z_{eff} = \frac{\sigma_a}{\sigma_e} , \tag{6}$$

where σ_a *(in* cm^2/gm*) is* the total atomic cross-sections [13], and σ_e*(in* cm^2/gm*) is* the total electronic cross-sections [32]

Besides, N_{eff} (in electrons/kg) is the effective number of electrons that defined as [33]:

$$N_{eff} = \frac{N_A}{N} Z_{eff} \sum_j n_j = \frac{\mu_m}{\sigma_e} , \tag{7}$$

where $\sum n_j$ is the total number of elements in the material Effective conductivity (C_{eff}; in S/m) is expressed as [34]:

$$C_{eff} = \left(\frac{N_{eff} \rho e^2 \tau}{m_e}\right) 10^3 , \tag{8}$$

where m_e (in *kg*) and *e* (*in Coulomb*) are mass and charge of the electron, respectively, τ (in sec) is the mean lifetime of the electron at the Fermi Surface.

The Energy exposure and absorption buildup factors (*EBF* and *EABF*) are two factors satisfy the case of non-focusing beam of photon energy that Beer-Lambert law is moderated. The relations and discussions of EBF and EABF are wildly explained in the literatures [35, 36], where their calculations are based on the equivalent atomic number Z_{eq}. Z_{eq} is a single parameter used to define the properties of materials concerning equivalent elements. Z_{eq} can be evaluated from the ratio of the Compton partial mass attenuation coefficient relative to the total mass attenuation coefficient at a certain energy of the photon, as follows [35, 36]:

$$Z_{eq} = \frac{Z_1\left(\log R_2 - \log R\right) + Z_2\left(\log R - \log R_1\right)}{\log R_2 - \log R_1}, \tag{9}$$

where Z_1 and Z_2 are the atomic numbers of the elements corresponding to the ratios R_1 and R_2, respectively and R is the ratio of mass attenuation coefficient due to Compton effect to the mass attenuation coefficient due to the total processes for the selected glasses at a certain energy.

The neutrons that have not any charge, interact with the material across several processes. These processes are nuclear fission, elastic and inelastic scattering, neutron capture and nuclear spallation. The fast neutron removal cross section (FNRCS) (ΣR) is a factor that is commonly used to evaluate the neutrons attenuation ability of a certain material. FNRCS is defined as:-

$$\sum R = \sum_i \rho_i \left(\sum R/\rho\right)_i \tag{10}$$

Here, ρ_i *is* the partial density and $(\Sigma R/\rho)_i$ is the mass removal cross section (MRCS) of the ith constituent element, respectively [37]. MRCS were gotten in accordance with the literatures [38, 39]

4. Results and discussion

Fig. 1 shows the variation of LAC values against photon energies for the investigated system. LAC has higher values at the low photon energies, which attributed to the K-absorption edge of the involved elements [40] (as shown in table 2). LAC is then decreased dramatically, it shows an exponential behavior in the medium photon energy range, and it has a nearly constant values at the high photon energies. LAC increases with the increasing of Pb doping ratio in the photon energy ranges despite (this change is relatively small to the diagram scale).

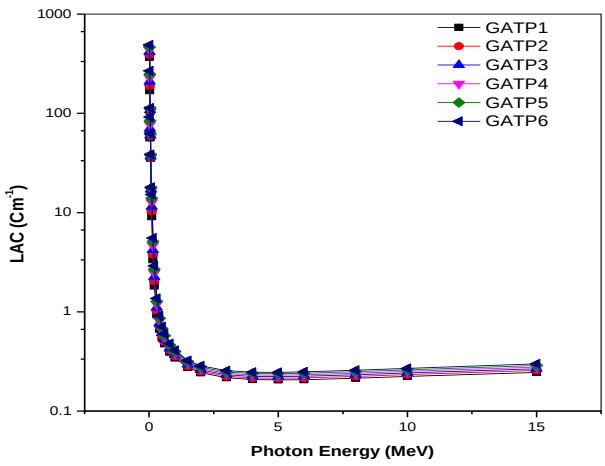

Fig. 1. LAC of the tested glasses (GATP1-GATP6) against photon energies (0.015 - 15 MeV).

Table 2. The atomic number Z and the absorption edges (MeV) of the constituent elements under investigation [40].

Element	Z	L3	L2	L1	K
Ge	32	1.217E-03	1.248E-03	1.414E-03	1.1103E-02
As	33	1.32310E-03	1.35860E-03	1.52650E-03	1. 18667E-02
Te	52	4.34140E-03	4.61200E-03	4.93920E-03	3.18138E-02
Pb	82	1.30352E-02	1.52E-02	1.58608E-02	8.80045E-02

It is well known that high monoenergetic photons interact with the material relying on the sample's atomic number (Z) and the incident photons' energy *E* in various dominant interaction processes at various energy ranges. Compton scattering (CS), and pair production (PP) are the most probable to occur at low, intermediate, and high, photoelectric absorption (PE). Therefore, the *LACs* of the various compositions under study have high values in the energy region where the photoelectric effect is dominant. The investigated specimens are almost having higher values of LAC than other commercial glasses and this indicate the possibility of using the investigated samples for better shielding against harmful radiations (see table 3)[41].

Table 3. LAC (in Cm^{-1}) of the investigated materials (GATP1-GATP6) versus some commercial glasses at various photon energies (in MeV) [41].

Energy in MeV	LAC (Cm^{-1})	RS-253	RS 253-G18	RS 323-G19	RS-360	RS-520	GATP1	GATP2	GATP3	GATP4	GATP5	GATP6
0.2		0.32	0.33	1.25	1.72	3.54	1.819	2.03125	2.24634	2.46338	2.683	2.904
0.662		0.19	0.19	0.28	0.32	0.5	0.472	0.486	0.499	0.513	0.527	0.542
1.25		0.14	0.14	0.18	0.21	0.3	0.313	0.321	0.330	0.340	0.349	0.359

MAC as function in photon energy has the same behavior (Fig 2) as LAC as function in photon energies. Fig 2 can be discussed in the same way of the above-mentioned dominant interaction processes. MAC varies in the range (71- 0.043 Cm^2/gm) in GATP6 and in the range (61-0.041 Cm^2/gm) in GATP1 as the photon energies change in between 0.015 and 15 MeV. Upon previous work [42, 43], we can say that *LAC* and *MAC* of our studied glasses are larger, consequently are better for shielding than some other traditional glasses as basalt- magnetite, steel-scrap, ilmenite-limonite, hematite-serpentine, ilmenite, steel-magnetite, and concretes [42,43].

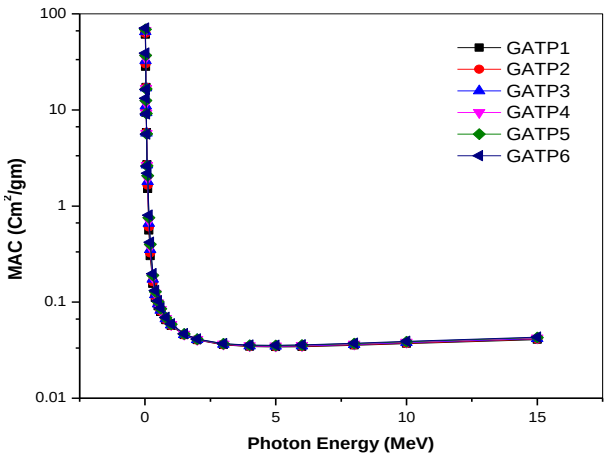

Fig. 2. MAC of the studied glasses (GATP1-GATP6) versus photon energies (0.015 - 15 MeV).

Figures 3, 4 show *HVL* and *TVL* variations as functions of photon energies (0.015-15 MeV). These graphs illustrate that *HVL* (0.00189-0.00142 Cm) and *TVL* (0.00627-0.0047 Cm) (for GATP1-GATP6) have their lowest values at the lowest photon energy (0.015 MeV). *HVL* and *TVL* increases rapidly until reaching 2 MeV, followed by a slowly increasing in the intermediate region of photon energy. *HVL* and *TVL* behavior being constant in the higher energies up to 15 MeV. These HVL and TVL behavior are attributed to the three basic processes of photon interactions with medium: PE, CE, and PP.

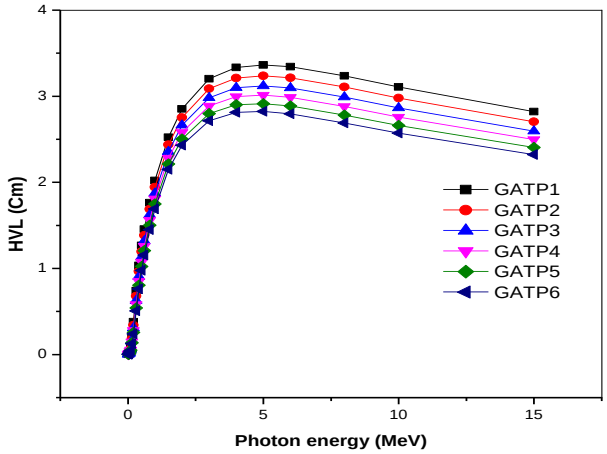

Fig. 3. HVL of the investigated chalcogenide glasses (GATP1-GATP6) as a function of photon energies (0.015 - 15 MeV).

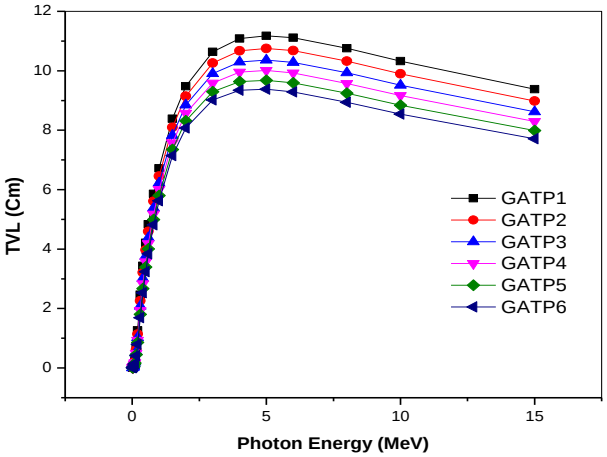

Fig. 4. TVL of (GATP1-GATP6) glasses versus photon energies (0.015 - 15 MeV).

The results declare that the GATP6 has the lowest values of *HVL* and *TVL* especially at almost medium and high photon energies (2-15 MeV). The addition of Pb to the (GATP1-GATP6) chalcogenide glasses enhance the shielding coefficients specifically at the medium and high photon energies, since Pb has higher density and atomic number in comparison with Te (Pb is substituted by Te in the studied glasses).

Figure 5 illustrates the MFP plot against photon energy (0.015-15 MeV). It is obviously shown that MFP has the same behavior of that of HVL and TVL.

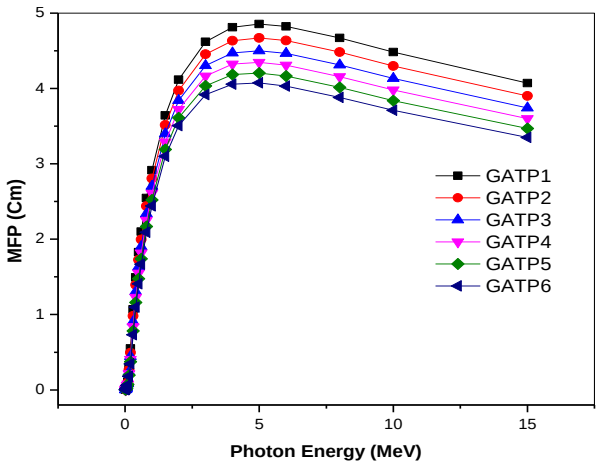

Fig. 5. MFP of (GATP1-GATP6) tested glasses against photon energies (0.015 - 15 MeV).

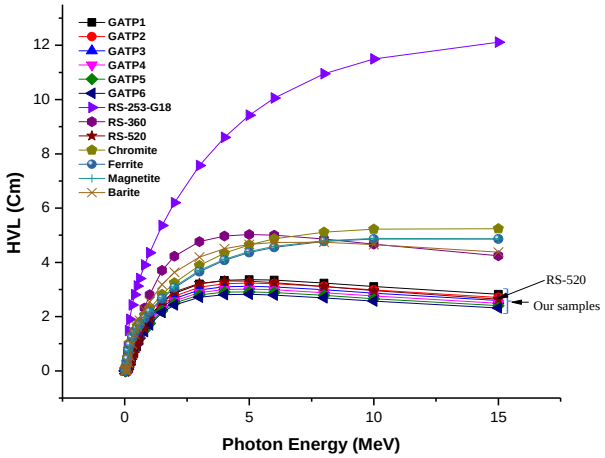

Fig. 6. HVL of (GATP1-GATP6) glasses and some ordinary and commercial glasses versus photon energies (0.015 - 15 MeV).

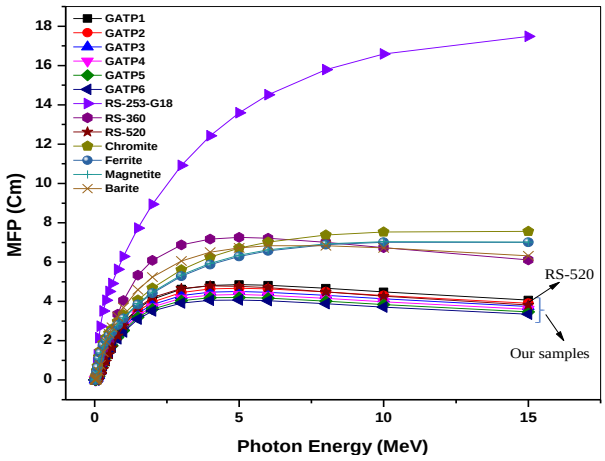

Fig. 7. MFP of (GATP1-GATP6) glasses under investigation and some traditional and commercial glasses against photon energies (0.015 - 15 MeV).

Figures 6 and 7 show comparisons between HVL and MFP of GATP glasses and other commercial and ordinary glasses [13]. These plots show that HVL and MFP of the investigated chalcogenide glasses GATP have lower values than all the ordinary glasses (Chromite, Ferrite, Magnetite and Barite) and all commercial glasses (RS-360-RS-253-G18-RS-520). At lower photon energies (0.015-0.03 MeV) RS-520 have lower values than all GAPT glasses. These results confirm a good competition of GATP glasses under investigation for better shielding purposes.

It is known that high values of ACS and ECS point to good quality of radiation shielding. Figures (8, 9) represent ACS and ECS respectively of GATP investigated glasses versus photon energy (0.015-15 MeV). ACS and ECS have their highest values at the lowest photon energies. ACS changes between 1.37E-20 and 8.38 E-24 Cm^2/gm, also ECS changes between 2.84E-22 and1.64E-25 cm^2/gm in GATP6 for example (the rest specimens take almost similar values). The trend behavior of ECS and ACS plots of GATP glasses can be clarified relying on the main interaction processes, PE, CE and PP.

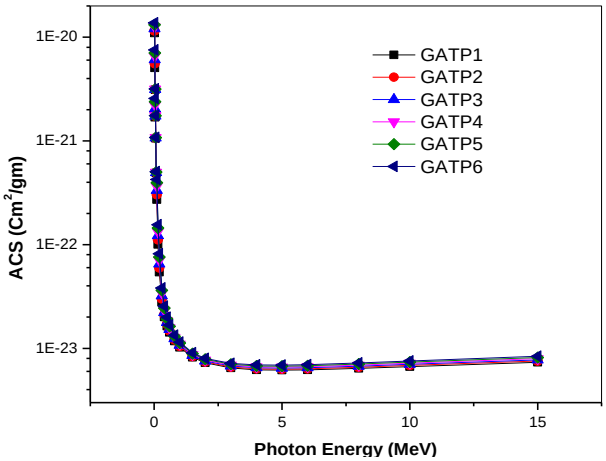

Fig. 8. ACS of (GATP1-GATP6) glasses as a function of photon energies (0.015 - 15 MeV).

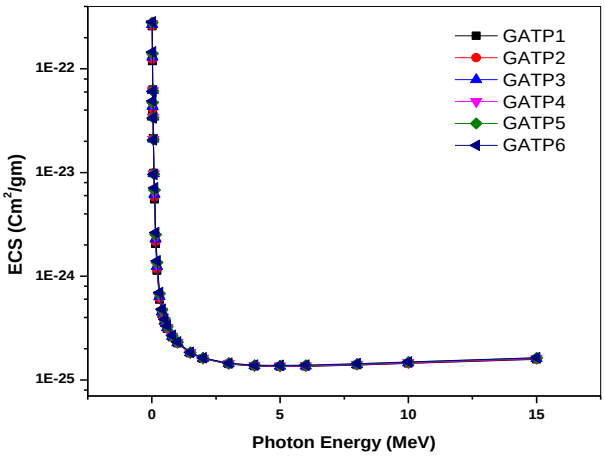

Fig. 9. ECS of the selected glasses (GATP1-GATP6) against photon energies (0.015 - 15 MeV).

Figure10 represents Z_{eff} of GATP glasses against photon energy. Z_{eff} for the tested specimens have their lowest values at 0.015 MeV. Z_{eff} have their highest values (59.75 -49.33) at 0.1 MeV for GATP1-GATP6 glasses. It is clearly confirmed that the compositions with higher doping of lead have higher values of Z_{eff} at the photon energy range, which indicate enhancing the

shielding characteristic of the material. Hence the higher values of Z_{eff} means reducing the photon energy crossing the medium.

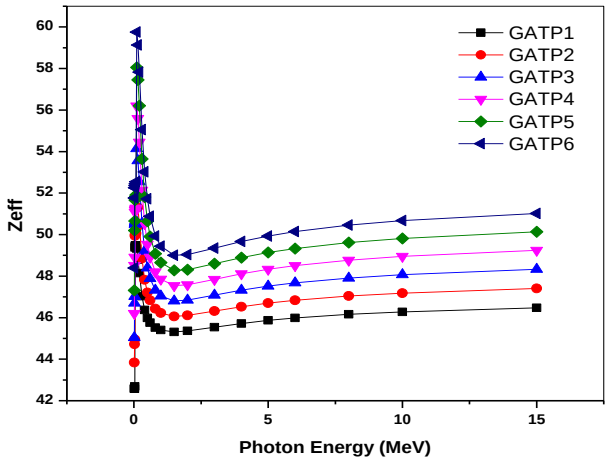

Fig. 10. Z_{eff} of (GATP1-GATP6) studied glasses versus energies (0.015 - 15 MeV).

Besides, N_{eff} and C_{eff}, which are dependent on Z_{eff}, are displayed as a function of photon energy, in figures 11 and 12 respectively. According to these graphs, N_{eff} and C_{eff} have similar behaviors of Z_{eff}.

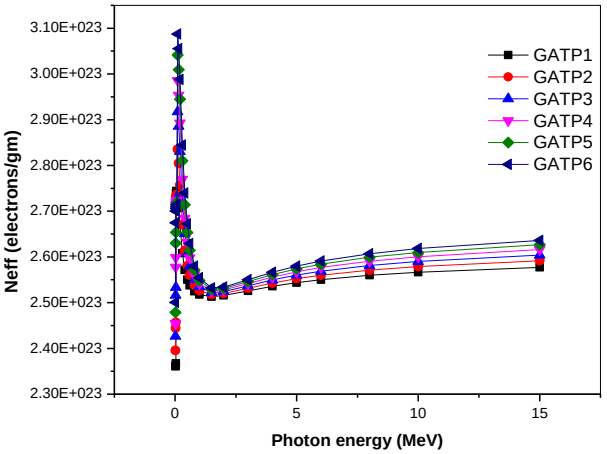

Fig. 11. N_{eff} of the (GATP1-GATP6) studied glasses against photon energies (0.015 - 15 MeV).

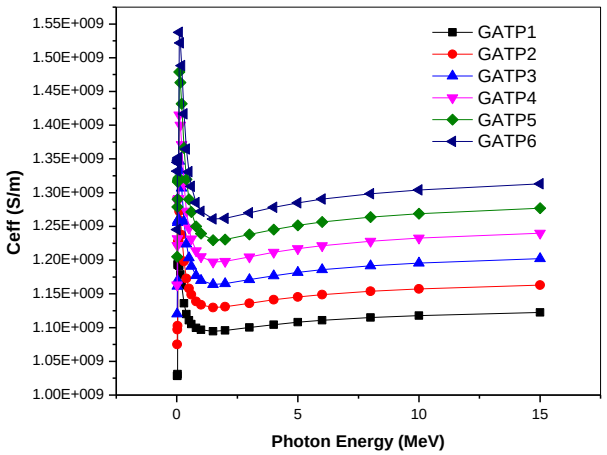

Fig. 12. C_{eff} of (GATP1-GATP6) with photon energies (0.015 - 15 MeV).

R coefficient of GATP investigated compositions are represented in figure 13 as a function of photon energy (0.015-15 MeV). The plot shows that the highest value of *R* is located at the medium energy region at 1.5 MeV, where the CE is the more dominant process. Figure 14 displays Z_{eq} parameter versus photon energies. Z_{eq} has its lowest values at 0.015 MeV and it increases rapidly until achieving their maximum values at 1 MeV (Z_{eq} = 58.12 for GATP6). Then, the plots drop gradually until being almost constant at the high energy region. The samples of higher ratio of lead have higher values of Z_{eq} at the entire photon energies range, that GATP6 have the highest Z_{eq} at all photon energies.

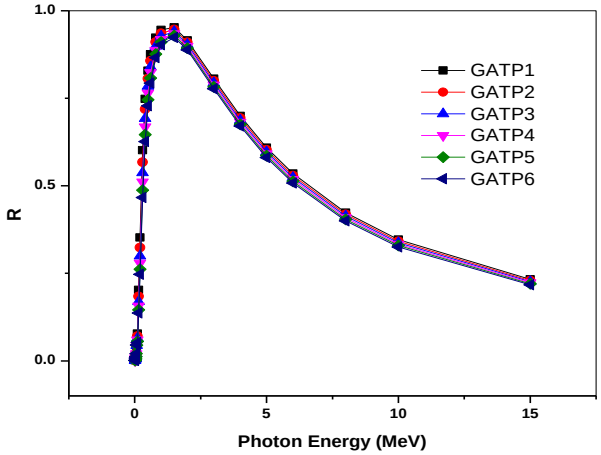

Fig. 13. R of the various (GATP1-GATP6) glasses under study versus photon energies (0.015 - 15 MeV).

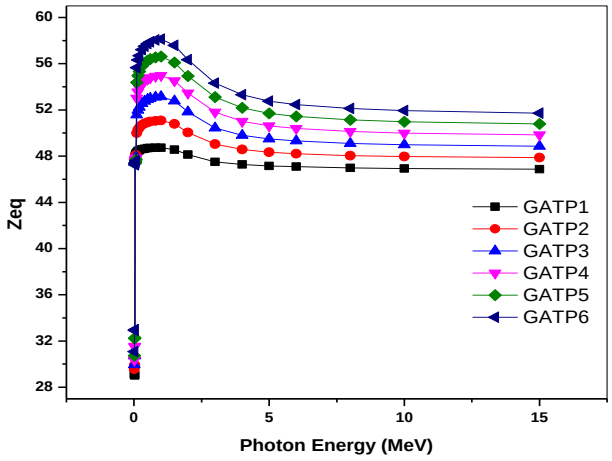

Fig. 14. Z_{eq} of (GATP1-GATP6) glasses against photon energies (0.015 - 15 MeV).

EBF and EABF are represented as a function of photon energy at different MFP (0.5 - 40). Figures 15 (a-c) and figures 16 (a-c) displayed the EBF and EABF of (GATP1, GATP3, GATP6), respectively. The curves show that EBF and EABF increase with increasing MFP at the entire photon energy for all the tested compositions. At 0.03 MeV, *EFB* and EABF being maximum for all values of MFP for all GATP glasses. The lowest values of EBF and EABF are at 0.015, 0.02 and 0.1 MeV (across *K*-absorption edges of the participating elements; Ge, As, Te, Pb). The lowest values of EBF and EABF can be discussed based on occurrence possibility of different photon interaction processes. Consequently, EABF and EBF were lowered. EBF and EABF increase at the intermediate region of photon energies (where, the CE is the most effective process), due to the improving of the photon dispersing process. Subsequently, the photon lifetime rises, which enhances its ability to wander from the substance. Also, EBF and EABF display another rising in a

higher photon energy (6 - 15 MeV) which assigned to the multiple scattering processes that improve the growth of secondary gamma photons due to electron-positron annihilation.

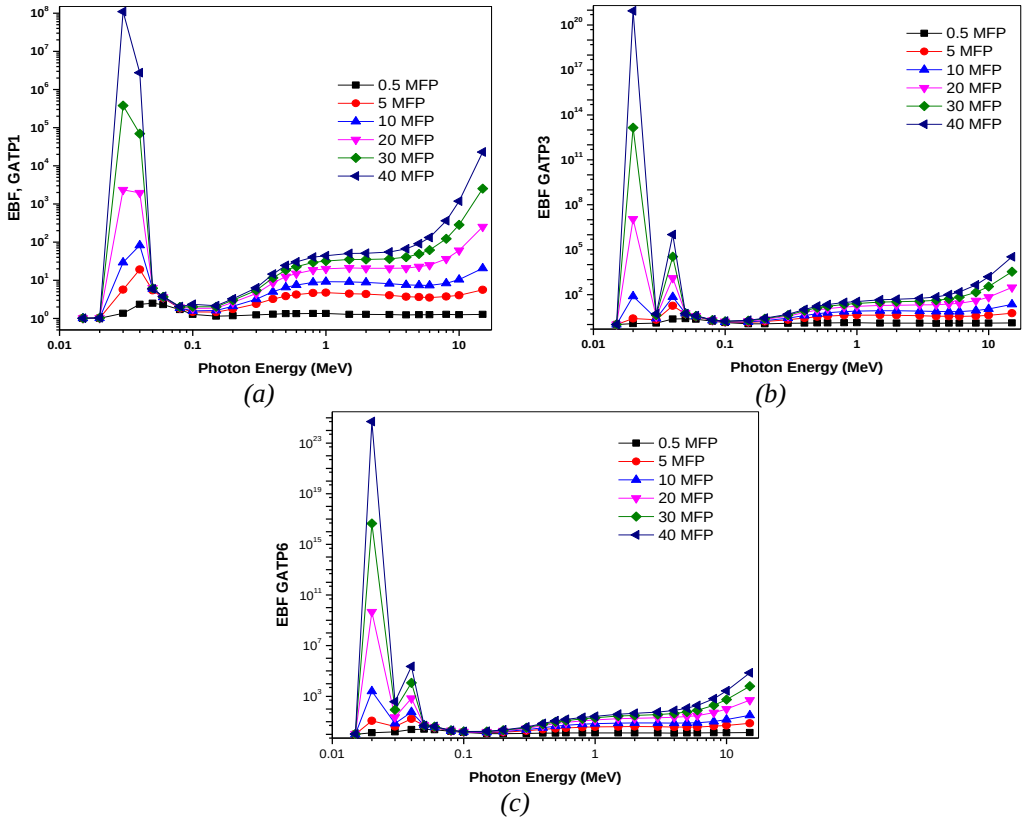

Fig. 15. (a-c) EBF of the (GATP1-GATP6) glasses as a function of photon energies (0.015 - 15 MeV).

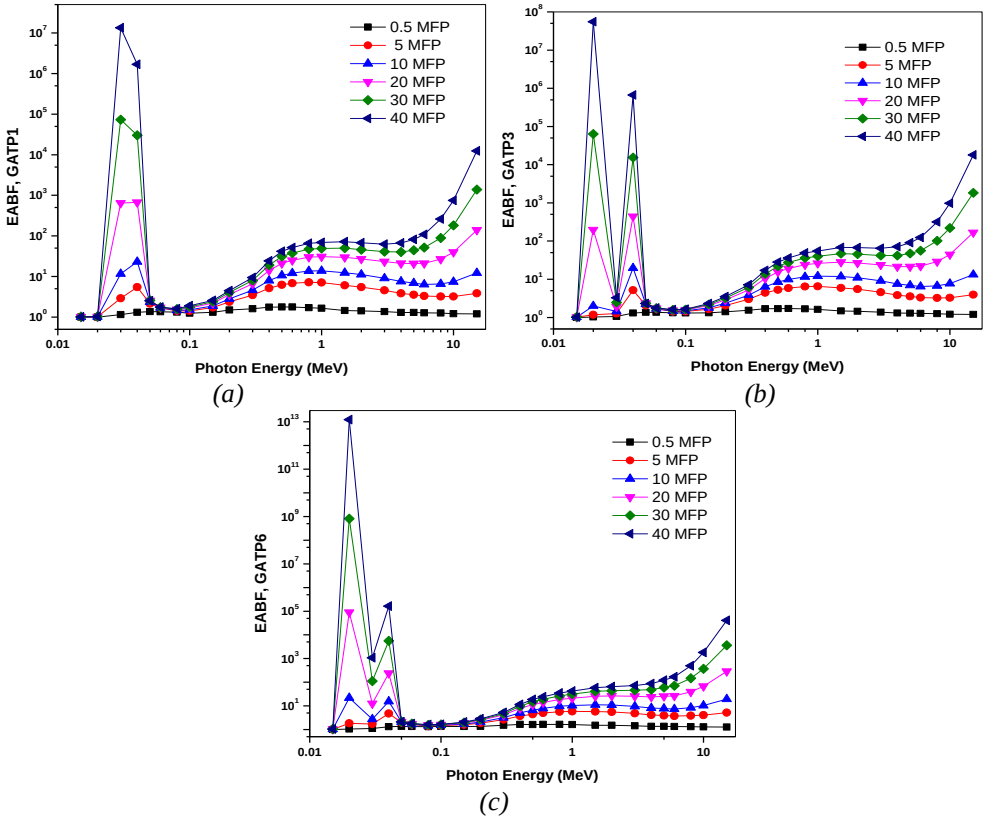

Fig. 16. (a-c) EABF of (GATP1-GATP6) glasses against photon energies (0.015 - 15 MeV).

It is noticeable that EBF and EABF reduce with increasing Pb content within the studied samples at entire range of photon energy at all MFP values, which emphasize the enhancement of radiation shielding quality with the addition of Lead to the tested specimens.

The measured values of FNRCS of the GATP compositions under investigation compared with other commercial and ordinary glasses are obviously shown in figure 17 [13]. FNRCS values (GATP1, GATP2, GATP3, GATP4, GATP5) were (0.087, 0.089, 0.09, 0.092, 0.094, 0.095 Cm^{-1}) respectively. The plot show that FNRCS of GATP1-GATP6 glasses are superior and consequently better than all the commercial glasses shown in the graph (RS-360, RS-253-G18, RS-520), but they are lower than all the mentioned ordinary glasses (Chromite, Ferrite, Magnetite, Barite). Indeed, Pb improves the shielding capability of the studied GATP samples by rising FNRCS, which ascribed to the greater atomic number and the greater density of Pb compared with that of Te.

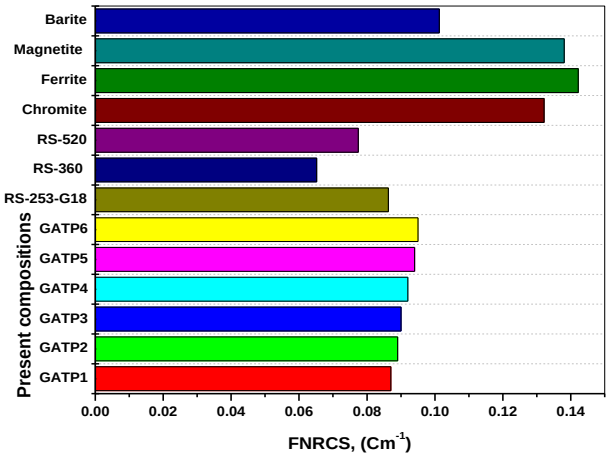

Fig. 17. FNRCS of (GATP1-GATP6) glasses in comparison with FNRCS of some ordinary and commercial glasses.

5. Conclusion

Shielding of high energetic radiations for different compositions of Ge_{25}-As_{10}-Te_{65-x}-Pb_x (x = 0, 2, 4, 6, 8, 10 at %) have been investigated in accordance with Phy-X/PSD program at photon energies, which varies between 0.15 and 15 MeV. The results asserted that the investigated specimens are almost having higher values of LAC than other commercial glasses and this indicates the possibility of using the investigated samples for better shielding against harmful radiations. HVL, TVL, and MFP were reduced with rising Pb doping rates in the tested compositions. HVL and MFP of the investigated chalcogenide glasses have lower values than all the mentioned ordinary and commercial glasses except at lower photon energies (0.015-0.03 MeV) RS-520 have lower values than all the tested glasses and lower values in the hole photon energies than GATP1(as mentioned earlier). Z_{eff}, C_{eff}, N_{eff}, Z_{eq} were found to rise with rising Pb contents in the tested specimens that were ascribed to its great atomic number and density. EBF and EABF measurements showed growing trend with rising MFP at the entire photon energy range, but these values were reduced with rising Pb doping ratio in the studied glasses at the whole photon energy region. FNRCS are changed between 0.087 and 0.095 Cm^{-1} as the Pb doping ratio within the tested glasses varies between 0.0 and 0.01 respectively. These results confirm a good competition of GATP glasses under investigation for better shielding purposes than many of ordinary and commercial glasses.

Acknowledgments

This work was funded by the Deanship of Scientific Research at Jouf University under grant No (DSR-2021-03-0391).

References

[1] V. Singh, S. Shirmardi, M. Medhat, and N. Badiger, "Determination of mass attenuation coefficient for some polymers using Monte Carlo simulation," Vacuum, vol. 119, pp. 284-288, 2015; https://doi.org/10.1016/j.vacuum.2015.06.006

[2] J. Singh, H. Singh, J. Sharma, T. Singh, and P. S. Singh, "Fusible alloys: a potential candidate for gamma rays shield design," Progress in Nuclear Energy, vol. 106, pp. 387-395, 2018; https://doi.org/10.1016/j.pnucene.2018.04.002

[3] M. Sayyed, G. Lakshminarayana, I. Kityk, and M. Mahdi, "Evaluation of shielding parameters for heavy metal fluoride based tellurite-rich glasses for gamma ray shielding applications," Radiation Physics and Chemistry, vol. 139, pp. 33-39, 2017; https://doi.org/10.1016/j.radphyschem.2017.05.013

[4] K. Mahmoud, M. Sayyed, and O. Tashlykov, "Gamma ray shielding characteristics and exposure buildup factor for some natural rocks using MCNP-5 code," Nuclear Engineering and Technology, vol. 51, pp. 1835-1841, 2019; https://doi.org/10.1016/j.net.2019.05.013

[5] Asmaa Mansour, M I Sayyed, K A Mahmoud, Erdem Şakar & E G Kovaleva, Modified halloysite minerals for radiation shielding purposes, Journal of Radiation Research and Applied Sciences, 13:1, 94-101, 2020; https://doi.org/10.1080/16878507.2019.1699680

[6] Y. Rammah, K. Mahmoud, M. Sayyed, F. El-Agawany, and R. El-Mallawany, "Novel vanadyl lead-phosphate glasses: P2O5-PbO-ZnONa2O-V2O5: Synthesis, optical, physical and gamma photon attenuation properties," Journal of Non-Crystalline Solids, vol. 534, p. 119944, 2020; https://doi.org/10.1016/j.jnoncrysol.2020.119944

[7] K. A. Mahmoud, O. L. Tashlykov, A. F. E. Wakil, H. M. H. Zakaly, and I. E. E. Aassy, "Investigation of radiation shielding properties for some building materials reinforced by basalt powder," AIP Conference Proceedings, vol. 2174, p. 020036, 2019; https://doi.org/10.1063/1.5134187

[8] A. Aşkın, "Assesment of the gamma and neutron shielding capabilities of the boro-tellurite glass quaternary containing heavy metal oxide using Geant4 and Phy-X/PSD database," Ceramics International, 2020; https://doi.org/10.1016/j.ceramint.2020.02.209

[9] K. Mahmoud, E. Lacomme, M. Sayyed, Ö. Özpolat, and O. Tashlykov, "Investigation of the gamma ray shielding properties for polyvinyl chloride reinforced with chalcocite and hematite minerals," Heliyon, vol. 6, p. e03560, 2020; https://doi.org/10.1016/j.heliyon.2020.e03560

[10] A. Kumar, D. Gaikwad, S. S. Obaid, H. Tekin, O. Agar, and M. Sayyed, "Experimental studies and Monte Carlo simulations on gamma ray shielding competence of (30+ x) PbO10WO3 10Na2O− 10MgO-(40-x) B2O3 glasses," Progress in Nuclear Energy, vol. 119, p. 103047, 2020; https://doi.org/10.1016/j.pnucene.2019.103047

[11] H. Tekin, L. Kassab, S. A. Issa, M. Martins, L. Bontempo, and G. R. da Silva Mattos, "Newly developed BGO glasses: synthesis, optical and nuclear radiation shielding properties," Ceramics International, 2020; https://doi.org/10.1016/j.ceramint.2020.01.221

[12] B. Alım, "A comprehensive study on radiation shielding characteristics of Tin-Silver, Manganin-R, Hastelloy-B, Hastelloy-X and Dilver-P alloys," Applied Physics A, vol. 126, pp. 1-19, 2020; https://doi.org/10.1007/s00339-020-3442-7

[13] E. Şakar, Ö. F. Özpolat, B. Alım, M. Sayyed, and M. Kurudirek, "Phy-X/PSD: development of a user friendly online software for calculation of parameters relevant to radiation shielding and dosimetry," Radiation Physics and Chemistry, vol. 166, p. 108496, 2020; https://doi.org/10.1016/j.radphyschem.2019.108496

[14] A. Abouhaswa, M. Al-Buriahi, M. Chalermpon, and Y. Rammah, "Influence of ZrO 2 on

gamma shielding properties of lead borate glasses," Applied Physics A, vol. 126, pp. 1-11, 2020; https://doi.org/10.1007/s00339-019-3264-7

[15] G. Lakshminarayana, M. Dong, M. Al-Buriahi, A. Kumar, D.-E. Lee, J. Yoon, et al., "B 2 O 3-Bi 2 O 3-TeO 2-BaO and TeO 2-Bi 2 O 3-BaO glass systems: a comparative assessment of gamma-ray and fast and thermal neutron attenuation aspects," Applied Physics A, vol. 126, pp. 1-18, 2020; https://doi.org/10.1007/s00339-020-3372-4

[16] M. Kamislioglu, E. A. Guclu, and H. Tekin, "Comparative evaluation of nuclear radiation shielding properties of x TeO 2+(100-x) Li 2 O glass system," Applied Physics A, vol. 126, pp. 1-16, 2020; https://doi.org/10.1007/s00339-020-3284-3

[17] F. El-Agawany, K. Mahmoud, E. Kavaz, R. El-Mallawany, and Y. Rammah, "Evaluation of nuclear radiation shielding competence for ternary Ge-Sb-S chalcogenide glasses," Applied Physics A, vol. 126, pp. 1-11, 2020; https://doi.org/10.1007/s00339-020-3426-7

[18] I. Boukhris, M. Al-Buriahi, H. Akyildirim, A. Alalawi, I. Kebaili, and M. Sayyed, "Chalcogenide glass-ceramics for radiation shielding applications," Ceramics International, 2020; https://doi.org/10.1016/j.ceramint.2020.04.281

[19] I. Kebaili, I. Boukhris, M. Al-Buriahi, A. Alalawi, and M. Sayyed, "Ge-Se-Sb-Ag chalcogenide glasses for nuclear radiation shielding applications," Ceramics International, vol. 47, pp. 1303-1309, 2020; https://doi.org/10.1016/j.ceramint.2020.08.251

[20] A. Srivastava, S. Sharma, and N. Mehta, "Characterization of novel SeTeSn Chalcogenide Glassy Alloy (STS ChGA) as shielding material: Case study of its resistance against γ-ray irradiation for nuclear waste immobilization applications," Journal of Environmental Chemical Engineering, vol. 7, p. 103032, 2019; https://doi.org/10.1016/j.jece.2019.103032

[21] S. A. Issa, H. Tekin, R. Elsaman, O. Kilicoglu, Y. B. Saddeek, and M. Sayyed, "Radiation shielding and mechanical properties of Al2O3-Na2O-B2O3-Bi2O3 glasses using MCNPX Monte Carlo code," Materials Chemistry and Physics, vol. 223, pp. 209-219, 2019; https://doi.org/10.1016/j.matchemphys.2018.10.064

[22] Y. Rammah, A. Askin, A. Abouhaswa, F. El-Agawany, and M. Sayyed, "Synthesis, physical, structural and shielding properties of newly developed B 2 O 3-ZnO-PbO-Fe 2 O 3 glasses using Geant4 code and WinXCOM program," Applied Physics A, vol. 125, p. 523, 2019; https://doi.org/10.1007/s00339-019-2831-2

[23] Y. Rammah, F. El-Agawany, and I. El-Mesady, "Evaluation of photon attenuation and optical characterizations of bismuth lead borate glasses modified by TiO 2," Applied Physics A, vol. 125, p. 727, 2019; https://doi.org/10.1007/s00339-019-3023-9

[24] Y. Rammah, M. Sayyed, A. Ali, H. Tekin, and R. El-Mallawany, "Optical properties and gamma-shielding features of bismuth borate glasses," Applied Physics A, vol. 124, p. 832, 2018; https://doi.org/10.1007/s00339-018-2252-7

[25] F. El-Agawany, E. Kavaz, U. Perişanoğlu, M. Al-Buriahi, and Y. Rammah, "Sm 2 O 3 effects on mass stopping power/projected range and nuclear shielding characteristics of TeO 2-ZnO glass systems," Applied Physics A, vol. 125, p. 838, 2019; https://doi.org/10.1007/s00339-019-3129-0

[26] Y. Al-Hadeethi, M. Sayyed, and Y. Rammah, "Investigations of the physical, structural, optical and gamma-rays shielding features of B2O3-Bi2O3-ZnO-CaO glasses," Ceramics International, vol. 45, pp. 20724-20732, 2019; https://doi.org/10.1016/j.ceramint.2019.07.056

[27] A. Kumar, D. Gaikwad, S. S. Obaid, H. Tekin, O. Agar, and M. Sayyed, "Experimental studies and Monte Carlo simulations on gamma ray shielding competence of (30+ x) PbO10WO3 10Na2O− 10MgO-(40-x) B2O3 glasses," Progress in Nuclear Energy, vol. 119, p. 103047, 2020; https://doi.org/10.1016/j.pnucene.2019.103047

[28] Y. Al-Hadeethi and M. Sayyed, "Radiation attenuation properties of Bi2O3-Na2O-V2O5-TiO2-TeO2 glass system using Phy-X/PSD software," Ceramics International, vol. 46, pp. 4795-4800, 2020; https://doi.org/10.1016/j.ceramint.2019.10.212

[29] Y. Al-Hadeethi, M. Sayyed, and O. Agar, "Ionizing photons attenuation characterization of quaternary tellurite-zinc-niobium-gadolinium glasses using Phy-X/PSD software," Journal of Non-Crystalline Solids, vol. 538, p. 120044, 2020; https://doi.org/10.1016/j.jnoncrysol.2020.120044

[30] M. Ahmad, K. A. Aly, A. Dahshan, M. M. Soraya and Yasser B. Saddeek, "Study of the physical properties of quaternary Ge-As-Te-Pb thin flms for technology applications", Applied Physics A, vol.126, 2020; https://doi.org/10.1007/s00339-020-03672-6

[31] D. F. Jackson and D. J. Hawkes, "X-ray attenuation coefficients of elements and mixtures," Physics Reports, vol. 70, pp. 169-233, 1981; https://doi.org/10.1016/0370-1573(81)90014-4

[32] I. Han and L. Demir, "Studies on effective atomic numbers, electron densities and mass attenuation coefficients in Au alloys," Journal of X-ray Science and Technology, vol. 18, pp. 39-46, 2010; https://doi.org/10.3233/XST-2010-0238

[33] I. Han and L. Demir, "Studies on effective atomic numbers, electron densities from mass attenuation coefficients in TixCo1− x and CoxCu1− x alloys," Nuclear Instruments and Methods in Physics Research Section B: Beam Interactions with Materials and Atoms, vol. 267, pp. 3505-3510, 2009; https://doi.org/10.1016/j.nimb.2009.08.022

[34] H. Manjunatha, "A study of gamma attenuation parameters in poly methyl methacrylate and Kapton," Radiation Physics and Chemistry, vol. 137, pp. 254-259, 2017; https://doi.org/10.1016/j.radphyschem.2016.01.024

[35] Y. Harima, "An approximation of gamma-ray buildup factors by modified geometrical progression," Nuclear Science and Engineering, vol. 83, pp. 299-309, 1983; https://doi.org/10.13182/NSE83-A18222

[36] ANSI/ANS-6.4.3. Gamma Ray Attenuation Coefficient and Buildup Factors for Engineering Materials. American Nuclear Society La Grange Park, IL, 1991

[37] Wood, J.I., 1982. Computational Methods in Reactor Shielding. Pergamon Press.

[38] Chilton, A.B., Faw, R.E., Shultis, J.K., Principles of Radiation Shielding. Prentice-Hall, Englewood Cliffs, 1984

[39] Kaplan, M.F., Concrete Radiation Shielding: Nuclear Physics, Concrete Properties,Design and Construction. Longman Scientific & Technical, 1989

[40] J. H. Hubbell, S. M. Seltzer, Tables Of X-Ray Mass Attenuation Coefficients And Mass Energy Absorption Coefficient 1 keV TO 20 MeV For Elements Z = 1 To 92 And 48 Additional Substance Of Dosimetric Interest, Nist Research Information Center, 1995; https://doi.org/10.6028/NIST.IR.5632

[41] SCHOTT; http://www.schott.com/advanced_optics/english/products/opticalmaterials/ special-materials/radiation-shielding-glasses/index.html. (Accessed at 15/7/2020)

[42] Bashter II, Calculation of radiation attenuation coefficients for shielding concretes,Annals of Nuclear Energy, vol. 24, pp. 1389-401, 1997; https://doi.org/10.1016/S0306-4549(97)00003-0

[43] K. I. Hussein et al, Optical and radiation shielding properties for novel glass material: TeO2/Nb2O5/Ta2O5/La2O3, Chalcogenide Letters, Vol 19, No 6, 2022, https://doi.org/10.15251/CL.2022.196.417